with 40 panels. Also shown is the result from thin wing, small-amplitude theory.[14] Apart from a mild transient in the first cycle, the results rapidly converge to a steady-state solution, and with use of Eq. (3), this is within 2.5% of the thin wing solution. The linear variation of potential on the first wake panel made the calculation relatively insensitive to the time step size.[12] With a Kutta condition in the form of Eq. (1), the lift coefficient values were underpredicted by about 30%.

Figure 2 shows the pressure distributions over the section for this motion at the nondimensional time $t_n = 20$: Fig. 2a is with the Kutta condition in the form of Eq. (1); Fig. 2b is with use of Eq. (3). At this time step, the wing is descending with a nosedown pitch and lift is in an upward direction. Use of Eq. (1) leads to a pressure coefficient difference at the trailing edge of about 0.17 and generally lower absolute values of the pressure coefficient (and lower circulation) compared with the calculation done using Eq. (3), which insures equality of pressure on upper and lower surfaces at the trailing edge. Pressure coefficient differences at the trailing edge varied over the range ± 0.3 for this calculation.

Large differences in the pressure coefficient at the trailing edge again became predominant when calculations were done for conditions where the angle of attack of the airfoil was large (above about 15 deg) over a portion of the cycle. However, in real flow, separation would occur in these conditions, so this does not cause a limitation on the method in practice.

Acknowledgment

Financial support for this work came from the Natural Sciences and Engineering Research Council of Canada.

References

[1]Katz, J., and Weihs, D., "Wake Rollup and the Kutta Condition for Airfoils Oscillating at High Frequency," *AIAA Journal,* Vol. 19, No. 12, 1981, pp. 1604–1606.

[2]Crighton, D. G., "The Kutta Condition in Unsteady Flow," *Annual Review of Fluid Mechanics,* Vol. 17, 1985, pp. 411–445.

[3]Poling, D. R., and Telionis, D. P., "The Response of Airfoils to Periodic Disturbances—The Unsteady Kutta Condition," *AIAA Journal,* Vol. 24, No. 2, 1986, pp. 193–199.

[4]Katz, J., and Plotkin, A., *Low Speed Aerodynamics: From Wing Theory to Panel Methods,* McGraw-Hill, New York, 1991.

[5]Bose, N., "A Time-Domain Panel Method for Analysis of Foils in Unsteady Motion as Oscillating Propulsors," *Eleventh Australasian Fluid Mechanics Conference,* Univ. of Tasmania, Hobart, Tasmania, 1992, pp. 1201–1204.

[6]Bose, N., "Propulsive Performance of Chordwise Flexible Oscillating Foils Using a Time-Domain Panel Method," *Second Canadian Marine Dynamics Conference,* Univ. of British Columbia, Vancouver, British Columbia, Canada, 1993, pp. 150–156.

[7]Morino, L., and Kuo, C.-C., "Subsonic Potential Aerodynamics for Complex Configurations: A General Theory," *AIAA Journal,* Vol. 12, No. 2, 1974, pp. 191–197.

[8]Maskew, B., "Prediction of Subsonic Aerodynamic Characteristics: A Case for Low Order Panel Methods," *Journal of Aircraft,* Vol. 19, No. 2, 1982, pp. 157–163.

[9]Moran, J., *An Introduction to Theoretical and Computational Aerodynamics,* Wiley, New York, 1984, pp. 269–271.

[10]Kerwin, J. E., Kinnas, S. A., Lee, J.-T., and Shih, W.-Z., "A Surface Panel Method for the Hydrodynamic Analysis of Ducted Propellers," *Transactions of the Society of Naval Architects and Marine Engineers,* Vol. 95, 1987, pp. 93–122.

[11]Yon, S., Katz, J., and Plotkin, A., "Effect of Airfoil (Trailing Edge) Thickness on the Numerical Solution of Panel Methods Based on the Dirichlet Boundary Condition," *AIAA Journal,* Vol. 30, No. 3, 1992, pp. 697–702.

[12]Kinnas, S. A., and Hsin, C.-Y., "Boundary Element Method for the Analysis of the Unsteady Flow Around Extreme Propeller Geometries," *AIAA Journal,* Vol. 30, No. 3, 1992, pp. 688–696.

[13]Hoshino, T., "Hydrodynamic Analysis of Propellers in Steady Flow Using a Surface Panel Method," *Journal of the Society of Naval Architects of Japan,* Vol. 165, June 1989, pp. 55–70.

[14]Lighthill, M. J., "Aquatic Animal Propulsion of High Hydromechanical Efficiency," *Journal of Fluid Mechanics,* Vol. 44, No. 2, 1970, pp. 265–301.

Three-Dimensional Closure of the Passage-Averaged Vorticity-Potential Formulation

Xudong Zhang,* André Garon,† and Ricardo Camarero‡
École Polytechnique de Montréal, Montréal, Québec H3C 3A7, Canada

Introduction

THE numerical simulation of three-dimensional flows in multistage turbomachines is a difficult subject due to highly rotational viscous effects, further complicated by the unsteady and aperiodic nature of the rotor-stator interaction. The full coupling between the stator and rotor is still not practical within current computational capabilities because of the extraordinary fineness required to capture the flow structure. Thus a reduction of the complexity, based on a simplification of the governing set of equations by appropriate modeling and approximation, is a sensible strategy.

Among such approaches, the through-flow or axisymmetric model has played an important role, and when iteratively coupled with blade-to-blade calculations it leads to a quasi-three-dimensional model.[1-3] The validity of this model is in general dependent on the flow configuration and the accuracy of the blade-to-blade information and empirical data. Numerous attempts for treating these blade-to-blade effects have been carried out[4-6] and such models have been widely used in many turbomachinery design systems.

Recently, fully three-dimensional models for multistage configurations have become an attractive strategy since it is believed that they can provide more accurate predictions than quasi-three-dimensional models. Adamczyk[7] has developed a powerful methodology using sophisticated averaging procedures for each blade row and sets of three-dimensional equations are solved sequentially row by row until a common axisymmetric flow solution is obtained. This approach has shown its advantages and flexibility to simulate flows through multistage turbomachines and to account for the unsteady and aperiodic effects,[8] but requires computer resources not commonly available. Another fast and efficient three-dimensional approach has been proposed by Denton[9] and Dawes[10] for Euler (with a special treatment of viscous effects) and Navier-Stokes equations, respectively. Both assumed that the flow is steady and periodic relative to each of the blade rows individually. The coupling or communication between the blade rows is performed on a mixing plane, which is located between the blade rows where the axisymmetric averaged flow properties are transferred from the upstream to the downstream blade row. This approach limits its ability to handle the variation along the streamwise direction across this mixing plane.

In this Note, a modified three-dimensional model for simulating the rotor-stator interaction flow is described. In this model, fully three-dimensional flows are computed individually in the rotor and stator blade rows. The coupling between blade rows is performed axisymmetrically, but in contrast to Dawes,[10] the axisymmetric properties are obtained using a passage-averaged through-flow calculation instead of averaging the three-dimensional solutions on the mixing plane. Furthermore, the source terms in the through-flow equations are evaluated directly from the three-dimensional solutions for

Received Dec. 31, 1992; revision received Aug. 4, 1993; accepted for publication Sept. 20, 1993.

*Research Associate, Department of Mechanical Engineering.
†Assistant Professor, Department of Mechanical Engineering.
‡Professor, Department of Mechanical Engineering.

each blade row, instead of using blade-to-blade solutions and empirical data. This approach is applied to steady incompressible Navier-Stokes equations based on vorticity-potential formulation. Preliminary computations are conducted for a single-stage mixed-flow pump to demonstrate the capability of the proposed model and numerical results are presented and compared to experimental data.

Governing Equations

Three-Dimensional Equations

The basic principle behind the vorticity-potential formulation is the splitting of the velocity field $V = (v^r, v^\theta, v^z)$ into its rotational and irrotational parts:

$$V = -\nabla\phi + \nabla \times A \tag{1}$$

where (r, θ, z) is the cylindrical coordinates, ϕ a scalar potential field satisfying Laplace's equation, and $A = (A^r, A^\theta, A^z)$ a solenoidal vector potential field. Clearly, Eq. (1) ensures that the continuity equation is satisfied. The complete set of the three-dimensional steady incompressible laminar flow equations can be written in the following vector form:

$$(V \cdot \nabla)W - (W \cdot \nabla)V = 1/Re(\nabla^2 W) \tag{2}$$

$$\nabla^2\phi = 0 \tag{3}$$

$$\nabla^2 A = -W \tag{4}$$

$$V = -\nabla\phi + \nabla \times A \tag{5}$$

where $W = (w^r, w^\theta, w^z)$ is the vorticity field and Re is the Reynolds number.

Through-Flow Equations

The passage-averaged through-flow equations can be obtained by integrating the three-dimensional equations along the tangential direction θ. An alternative form of these equations are given by

$$\bar{v}^r \frac{\partial}{\partial r}(B\bar{w}^\theta) + \bar{v}^z \frac{\partial}{\partial z}(B\bar{w}^\theta) - \frac{\bar{v}^r}{r}(B\bar{w}^\theta) - \frac{1}{r}\frac{\partial}{\partial z}(B\bar{v}^\theta\bar{v}^\theta)$$
$$= \frac{1}{Re}\left\{\frac{\partial}{\partial r}\left[\frac{1}{r}\frac{\partial}{\partial r}(rB\bar{w}^\theta)\right] + \frac{\partial^2}{\partial z^2}(B\bar{w}^\theta)\right\} + F_w^\theta \tag{6}$$

$$\frac{1}{r}\frac{\partial}{\partial r}\left[r\frac{\partial}{\partial r}(B\bar{\phi})\right] + \frac{\partial^2}{\partial z^2}(B\bar{\phi}) = F_\phi \tag{7}$$

$$\frac{\partial}{\partial r}\left[\frac{1}{r}\frac{\partial}{\partial r}(B\bar{A}^\theta)\right] + \frac{\partial^2}{\partial z^2}(B\bar{A}^\theta) = -B\bar{w}^\theta + F_A^\theta \tag{8}$$

$$\bar{v}^r \frac{\partial}{\partial r}(B\bar{v}^\theta) + \bar{v}^z \frac{\partial}{\partial z}(B\bar{v}^\theta) + \frac{\bar{v}^r}{r}(B\bar{v}^\theta)$$
$$= \frac{1}{Re}\left\{\frac{\partial}{\partial r}\left[\frac{1}{r}\frac{\partial}{\partial r}(rB\bar{v}^\theta)\right] + \frac{\partial^2}{\partial z^2}(B\bar{v}^\theta)\right\} + F_v^\theta \tag{9}$$

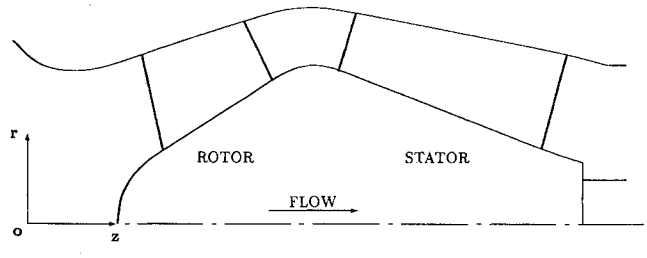

Fig. 1 Domain for the through-flow computation.

where B is the blockage parameter defined by $[N(\theta_s - \theta_p)]/2\pi$, with θ_s and θ_p the angular position of the suction and pressure surfaces of the blade, respectively, and

$$B\bar{v}^r = -\frac{\partial B\bar{\phi}}{\partial r} - \frac{\partial(B\bar{A}^\theta)}{\partial z} + F_v^r \tag{10}$$

$$B\bar{v}^z = -\frac{\partial B\bar{\phi}}{\partial z} - \frac{\partial(B\bar{A}^\theta)}{\partial r} + \frac{1}{r}(B\bar{A}^\theta) + F_v^z \tag{11}$$

In these equations, F_w^θ, F_ϕ, F_A^θ, F_v^θ, F_v^r, and F_v^z are the source terms detailed in Ref. 11, which are evaluated from the three-dimensional solutions obtained for each blade row individually. The overbar represents the averaged properties. The vorticity-potential formulation of the governing equations requires particular treatment of boundary conditions on potentials. The boundary conditions for the three-dimensional Eqs. (2–5) are given in Ref. 12 and the through-flow Eqs. (6–9) in Ref. 11. The main feature of the inlet and outlet boundary conditions for the potentials ϕ and $\bar{\phi}$ is to maintain the same mass flow. Body-fitted meshes and implicit finite-difference method were used to solve these equations.

Solution Procedure

The proposed model for the rotor-stator flow interaction consists of two sets of coupled equations. The three-dimensional Eqs. (2–5) are used for each blade row to provide three-dimensional flowfields, while the through-flow Eqs. (6–9) are solved throughout the machine to provide coupling information between the three-dimensional solutions.

In computing the through-flow field, the presence of the blades within the blade rows are accounted for by source terms whose values are deduced from the three-dimensional solutions within each blade row. To solve the three-dimensional equations, the required conditions are the inlet velocity distribution and the total mass rate at the exit. In the present study, since the flow is taken to be axisymmetric outside blade rows, the inflow velocity profile can be taken from the through-flow averaged solution. The data transfer from the three-dimensional to the through-flow equations and vice versa is repeated in the above manner until convergence is achieved.

Results and Discussions

The above calculation procedure was applied to the flow simulation in a single-stage mixed-flow pump with a five-blade rotor and a nine-blade stator. Details of the physical dimensions of the blades and a general description of the pump are given in Carey et al.[13] The meridional computational domain is shown in Fig. 1. It is noted that the rotor tip clearance was not considered in the present numerical simulation. A grid of 13×59 was used for the through-flow computation with 13 points in the radial direction, 15 points spaced uniformly in the circumferential direction for the rotor, and 13 points for the stator. The results are presented in terms of the velocity component V_p parallel to the streamwise grid line and the tangential velocity W_t in the relative rotating frame of reference compared with the measurements[13] performed in an air model of the machine at a shaft speed of 1200 rpm of the rotor. The experimental data for all velocities are normalized by the blade velocity at the rotor trailing-edge midspan, which is $U_t = 27$ m/s, corresponding to a Reynolds number of $Re = 1.5 \times 10^6$. However, since the model for the present study is for laminar flow, the Reynolds number for the numerical computation was set to 1500.

Figures 2 and 3 show the blade-to-blade velocity variations normalized by the distance from the suction to the pressure side. To show the streamwise evolution of the velocity components within the rotor, the blade-to-blade variations are given at midchord ($C = 0.5$) and near the rotor outlet with $C = 0.87$, where C is the normalized distance from the leading edge to trailing edge, and hub-to-shroud variations are given at $R = 0.167$, 0.5, 0.833, and 0.917, where R is the normalized

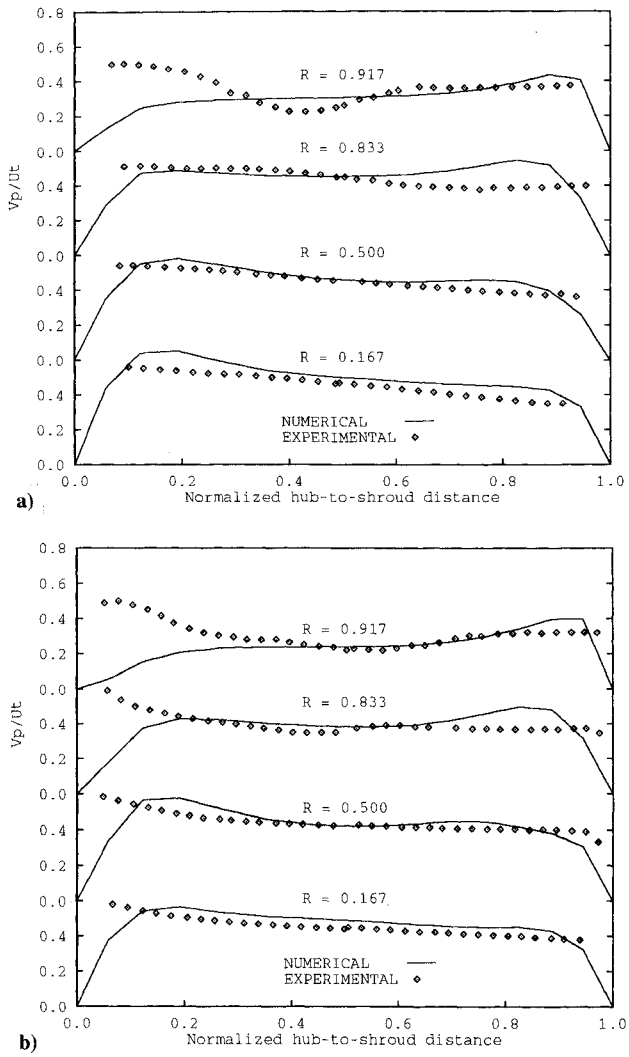

Fig. 2 Rotor blade-to-blade velocity components V_p: a) $C = 0.5$ and b) $C = 0.87$.

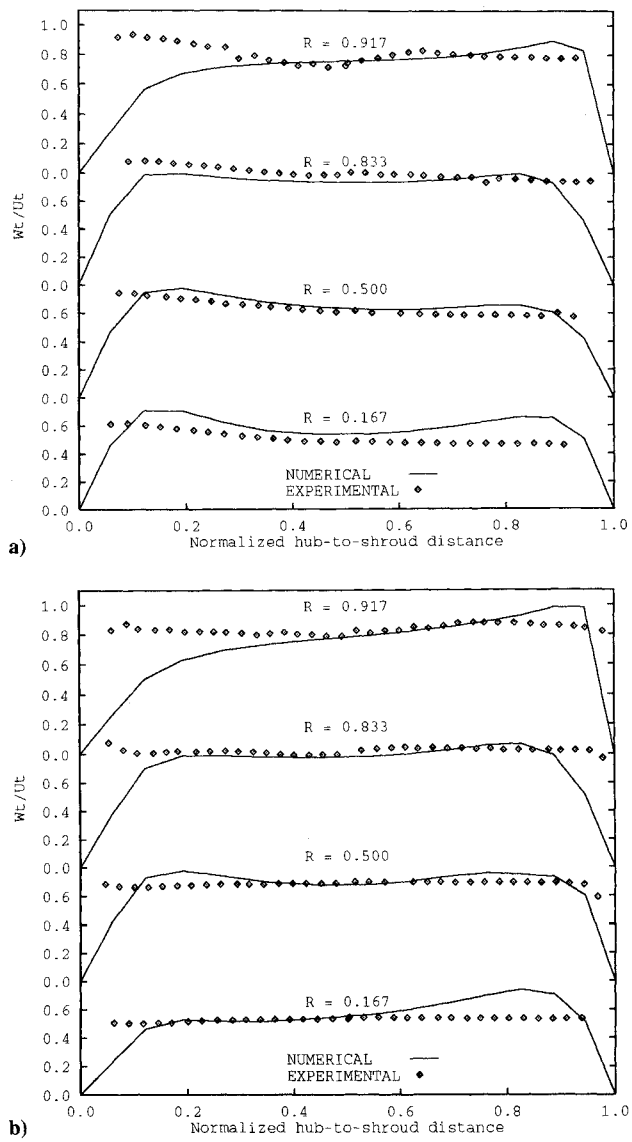

Fig. 3 Rotor blade-to-blade velocity components W_t: a) $C = 0.5$ and b) $C = 0.87$.

hub-to-shroud distance. In the mainstream flow region, the velocity components V_p (Fig. 2) show that the flow is accelerated near the blade suction surface and the relative tangential components W_t (Fig. 3) were decelerated near the suction surface and accelerated near the pressure surface. These observations agree well with the experimental data except at the edge of the blade surface boundary layers, where the velocities are relatively higher than the measured ones. This is expected since the Reynolds number for the computation is 1000 times lower than the experimental value. Consequently, a thicker boundary layer on the blade surface is observed which induces higher velocities at the edge of the boundary layer.

In the near shroud region ($R > 0.833$), complex turbomachinery flow phenomena are encountered. The blade boundary layers, the shroud boundary layer, the effects of the relative motion of the shroud, and the associated secondary flow interact to generate rapid changes in the fluid behavior. In Figs. 2 and 3, discrepancies between the predictions and the measurements for velocity components V_p and W_t appear. The main reason for such discrepancies is probably the absence of the blade-tip gap in the present numerical modeling.

Considering the absence of a proper turbulence model, the numerical results are reasonable and correctly represent the complex three-dimensional flow.

Acknowledgments

This work was supported by the National Science and Engineering Research Council of Canada (NSERC) and by Fonds pour la Formation de Chercheurs et l'Aide à la Recherche (FCAR) and Institut de Recherche d'Hydro-Québec (IREQ).

References

[1]Wu, C. H., "A General Theory of Three-Dimensional Flow in Subsonic and Supsonic Turbomachines of Axial, Radial and Mixed-Flow Types," NACA TN-2604, Jan. 1952.

[2]Jennions, I. K., and Stow, P., "A Quasi-Three-Dimensional Turbomachinery Blade Design System: Part I—Through-Flow Analysis," *ASME Journal of Engineering for Gas Turbines and Power,* Vol. 107, No. 2, 1985, pp. 301-308.

[3]Hirsch, Ch., and Deconinck, H., "Through-Flow Models in Turbomachines: Stream Surface and Passage-Averaged Representations," *Thermodynamics and Fluid Mechanics of Turbomachinery,* edited by A. Ş. Üçer, P. Stow, and Ch. Hirsch, NATO Advanced Science Institutes Series, Series E: Applied Sciences, No. 97A (Vol. 1), Martinus Nijhoff, Boston, 1985, pp. 73-129.

[4]Smith, L. H., Jr., "The Radial-Equilibrium Equation of Turbomachinery," *ASME Journal of Engineering for Power,* Vol. 88, No. 1, 1966, pp. 1-12.

[5]Bosman, C., and March, H., "An Improved Method for Calculating the Flow in Turbomachines Including a Consistent Loss Model," *Journal of Mechanical Engineering Science,* Vol. 16, No. 1, 1974, pp. 25-31.

[6]Sehra, A. K., and Kerrebrock, J. L., "Blade-to-Blade Flow Effects on Mean Flow in Transonic Compressors," *AIAA Journal,* Vol. 19, No. 4, 1981, pp. 476-483.

[7]Adamczyk, J. J., "Model Equation for Simulating Flows in Multistage Turbomachinery," NASA TM-86869, Nov. 1984.

[8]Mulac, R. A., and Adamczyk, J. J., "The Numerical Simulation of a High-Speed Axial Flow Compressor," *ASME Journal of Turbomachinery,* Vol. 114, No. 3, 1992, pp. 517-527.

[9]Denton, J. D., "The Calculation of Three-Dimensional Viscous Flow Through Multistage Turbomachines," *ASME Journal of Turbomachinery,* Vol. 114, No. 1, 1992, pp. 18-26.

[10]Dawes, W. N., "Toward Improved Throughflow Capability: The Use of Three-Dimensional Viscous Flow Solvers in a Multistage Environment," *ASME Journal of Turbomachinery,* Vol. 114, No. 1, 1992, pp. 8-17.

[11]Zhang, X., "Passage-Averaged Approximation of Turbomachinery Flow Using Vorticity-Potential Method," Ph.D. Thesis, Dept. of Applied Mathematics, École Polytechnique de Montréal, Canada, July 1991.

[12]Hirasaki, G. J., and Hellums, J. D., "Boundary Conditions on the Vector and Scalar Potentials in Viscous Three-Dimensional Hydrodynamics," *Quarterly of Applied Mathematics,* Vol. 28, No. 2, 1970, pp. 293-296.

[13]Carey, C., Fraser, S. M., Rachman, D., and Wilson, G., "Studies of the Flow of Air in a Model Mixed-Flow Pump Using Laser Doppler Anemometry," Technical Rept., National Engineering Lab. Rept. No. 698-699, Glasgow, Scotland, July 1985.

Asymptotic Probability Density Function of a Scalar

R. W. Derksen*
University of Manitoba,
Winnipeg, Manitoba R3T 2N2, Canada
P. J. Sullivan†
University of Western Ontario,
London, Ontario N6A 5B9, Canada
and
H. Yip‡
Department of National Defense,
Ottawa, Ontario K1A 0K2, Canada

Introduction

THERE are inherent difficulties in measuring contaminant statistics in general (see Derksen and Sullivan[1]) and conditional probabilities in specific (see Chatwin and Sullivan[2]). In Chatwin and Sullivan[3] an expression for the moments of the probability density function (PDF), given in Eq. (1), was shown to represent experimental data from a wide variety of turbulent shear flows. The data were taken at large enough downstream distances in these flows that the moments of the scalar concentration appeared to be self-similar. The objective here is to find the self-similar PDF of contaminant concentration that corresponds to those moments.

The asymptotic moments of the PDF are given in Chatwin and Sullivan[3] as

$$\mu_n' = \frac{\beta^n}{\alpha}\,\mu_1^n(0)[\chi(\alpha-\chi)^n + (-1)^n(\alpha-\chi)\chi^n] \qquad (1)$$

where $\chi = \mu_1(\eta)/\mu_1(0)$, $\eta = y/\ell = 0$ is evaluated at the location of the maximum mean concentration (the centerline of flows like jets and wakes and at the wall in boundary layers), and y is the cross-stream distance measured from this position with ℓ defined by $\mu_1(\ell) = \frac{1}{2}\mu_1(0)$. Here,

$$\mu_n = \int_0^\infty \theta^n p(\theta)\,d\theta, \qquad \mu_n' = \int_0^\infty (\theta-\mu_1)^n p(\theta)\,d\theta \qquad (2)$$

and

$$p(\theta) = \text{prob}(\theta \le \gamma < \theta + d\theta) \qquad (3)$$

is the PDF for scalar contaminant concentration θ. Equation (1) has the advantage that all of the central moments are expressed in terms of the mean concentration μ_1, which is the most easily measured and theoretically predicted statistic. That is, μ_1 is relatively insensitive to temporal and spatial measurement averaging and to the effects of molecular diffusivity. The distribution of lower ordered moments, at normally measured downstream distances, appears to be reasonably described by Eq. (1) over a wide range of flow conditions including jets, wakes, boundary layers, and plumes in grid turbulence. The range of the two parameters α and β that appear in Eq. (1) was found to be relatively narrow, i.e., $1 \le \alpha \le 1.5$ and $0.1 \le \beta \le 0.75$. In Derksen and Sullivan[1] the practical advantages of using measured lower ordered moments is discussed. There a Jacobi polynomial expansion, motivated by the structure of the lower ordered moments in Eq. (1), and also a maximum entropy formulation were used to invert measured moments to generate the PDF. The asymptotic moments given by Eq. (1) are not amenable to inversion using Jacobi polynomials; however, careful application of the maximum entropy formulation enables one to compile the asymptotic forms of the PDF.

Figures 1a-1f show the variation in the PDF over the cross section of a turbulent shear flow. The dominant features are two narrow peaks that correspond to the contributions to the scalar from the central (high-concentration) and peripheral (low-concentration) regions of the flow. The PDFs shown on Fig. 1 are consistent with the theoretical description of self-similar scalar PDFs within a turbulent shear flow that is developed in Chatwin and Sullivan[3] and which predicates on a separation of the time scales of long-term molecular diffusion and short-term local turbulent convective motions. A low-concentration peak progresses from a small magnitude at the center to virtually the entire PDF at the periphery of flows, whereas a high, dominant peak at the central region diminishes to insignificance in the peripheral regions. It is interesting to note in passing the proposal of Effelsberg and Peters,[4] and its discussion in Drake et al.,[5] to represent the PDF as a composite of a delta function (non-turbulent fluid), a Beta distribution (fully turbulent part), and an algebraic part for a transitional superlayer. The forms of the Beta distribution are Gaussian-like throughout. The disadvantages of that approach are discussed in Chatwin and Sullivan.[2]

It is of interest to compare the results shown in Fig. 1 with experimentally observed values presented in Antonia and Sreenivasan[6] (see also Dahm and Dimotakis[7]). There in a co-flowing, heated, round jet, scalar PDFs appeared to consist of a rather sharp spike near the nominal freestream temperature and a second much wider hump centered on higher values of temperature. The narrow low-temperature spike is of relatively small magnitude on the centerline and increases in magnitude, relative to the high-temperature mound, until it becomes the dominant feature of the PDF at the jet periphery. The two peaks are of equal magnitude at the approximate location of the mean temperature half-width. These observations of the low-temperature spike are certainly qualitatively similar to the distributions presented in Fig. 1 and the equal height of the two peaks at approximately the half-width location is observed in Fig. 1b. There is a significant difference between the observed high-temperature mound width and the corresponding narrow distribution shown on Fig. 1.

The inversion technique, whereby a finite number of moments given in Eq. (1) are used to compile the PDFs shown on Fig. 1, is described in Derksen and Sullivan.[1] Newton's

Received Dec. 24, 1992; revision received Oct. 24, 1993; accepted for publication Oct. 28, 1993.

*Assistant Professor, Department of Mechanical and Industrial Engineering.

†Professor, Department of Applied Mathematics.

‡Defence Scientist, Operational Research and Analysis Establishment, M. Gen. George R. Pearkes Bldg., 101 Colonel By Drive.